GFD 2017 Lecture 3: Subglacial Control of Ice Flow

Andrew Fowler; notes by Eric Hester and Jessica Kenigson

June, 21, 2017

1 Subglacial Floods: Grímsvötn

Jökulhlaups or "glacier-bursts" are flooding events that are associated with glaciers; these events may be quasi-periodic or periodic. In 1996, a massive Jökulhlaups occurred at the Skeiðarárjökull glacier at Iceland, which partially overlays a lake within a geothermally heated caldera. The ice overburden pressure at the caldera rim forms a "seal" which prevents the lake from emptying. Figure 1 shows a simplified geometric profile of the region.

Flooding events at Grímsvötn occur regularly, indeed quasi-periodically ($\sim$5-10 years) (Figure 2). A plausible mechanism for flooding from Grímsvötn would involve the water pressure in the lake growing to exceed the ice overburden pressure and causing flotation of the glacier, releasing a burst of water through the broken "seal." During observed flooding conditions, however, the water level within the lake has not been observed to reach the necessary height to achieve glacier flotation. A simplified physical model will be developed to shed light on the flow of water beneath the glacier during flood events as well as the periodicity of these events. Much of the following theory follows the exposition by [4].

1.1 Model

Water flows through a semi-circular conduit (i.e., a Röthlisberger Channel) of cross-sectional area S at the glacier base. In the Röthlisberger model, melting of the channel walls occurs through frictional heating via contact with the flowing water, and creep closure occurs because the ice overburden pressure exceeds the water pressure in the channel. That is, in general, $N = p_i - p_w > 0$. Equation 2 models the change in the cross-sectional area of the conduit under the competing effects of melting of the sidewalls m and creep closure SN^n. Therefore

$$\frac{\partial S}{\partial t} = \frac{m}{\rho_i} - KS(p_i - p_w)^n, \tag{1}$$

where subscripts i and w indicate ice and water, respectively, and K is a constant which depends upon the geometry of the conduit. The second term arises from the nonlinear flow law for plastic deformation. Two separate sources are assumed for volumetric flux Q to the channel: melt of the channel walls and other sources such as surface meltwater and outflow

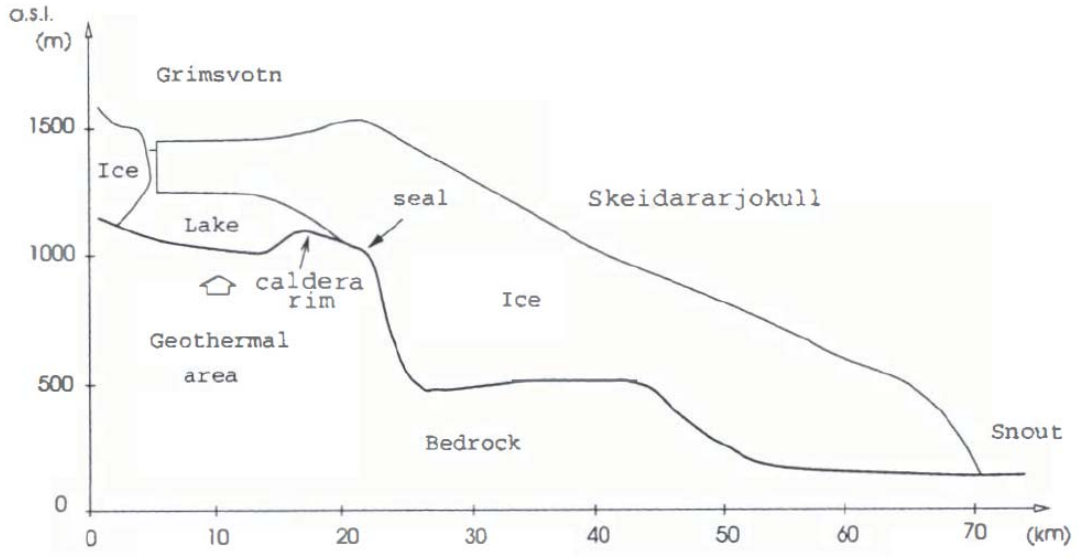

Figure 1: Simplified profile of the landscape near Grímsvötn. In the Röthlisberger-Nye model x is increasing to the right and is measured from the seal (which is assumed to be fixed in space). Figure from [1].

from the lake, which are subsumed into a single term M. Therefore, continuity of mass within the conduit implies

$$\frac{\partial S}{\partial t} + \frac{\partial Q}{\partial x} = \frac{m}{\rho_w} + M. \tag{2}$$

A momentum balance arises from rearranging the Gauckler-Manning formula for a mean (turbulent) flow $\bar{u} = Q/S$:

$$\bar{u} = \frac{R^{2/3}}{n'} \left[\frac{1}{\rho_w g} \left(\rho_w g_s - \frac{\partial p}{\partial s} \right) \right] \tag{3}$$

where R is the hydraulic radius, g is the gravitational constant, g_s is the component of the gravitational constant in the s-direction (here x-direction), n' is a Manning roughness factor, and ρ_w is the density of water [7]. It follows that

$$\rho_w g \sin\alpha - \frac{\partial p}{\partial x} = f \rho_w g \frac{Q\,|Q|}{S^{8/3}} \tag{4}$$

where the first term represents the gravitational driving force, the second term represents the water pressure gradient, and the third term represents bed friction. Here f is a friction factor and α is the bed inclination. Finally, the energy equation is

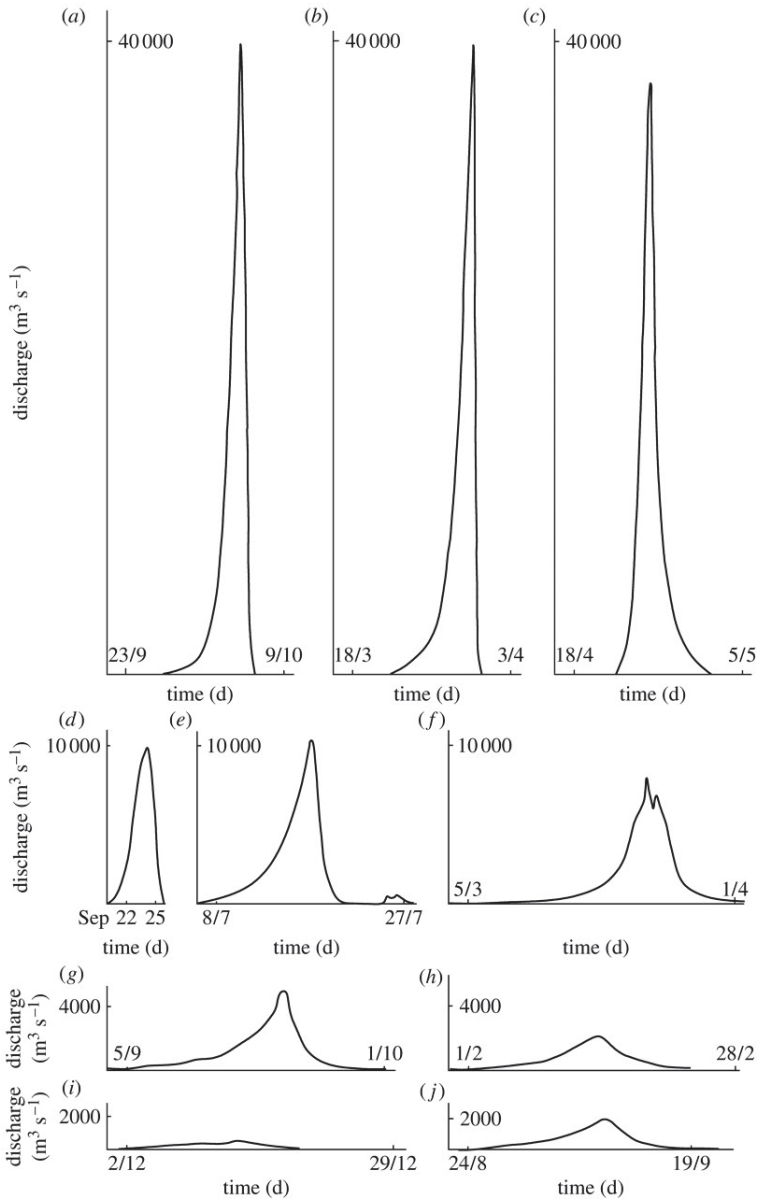

Figure 2: Hydrograph showing extreme flooding events at Grímsvötn in 1922, 1934, 1938, 1945, 1954, 1972, 1976, 1982, 1983, and 1986. Figure from [3].

$$\rho_w c_w \left[S\frac{\partial \theta_w}{\partial t} + Q\frac{\partial \theta_w}{\partial x} \right] = Q\left(\rho_w g \sin\alpha - \frac{\partial p}{\partial x} \right) - m\left[L + c_w(\theta_w - \theta_i) \right] \tag{5}$$

where the rate of change of internal energy is given by the sum of two terms: the energy needed to change the temperature of water already in the conduit (term related to the total derivative of θ_w on the LHS), and the energy needed to melt ice from the conduit walls (second term on the RHS), which consists of a sum of the energy required to raise the ice temperature to the water temperature and the latent heat needed for the phase change. The first term on the RHS is the frictional heating due to viscous dissipation (see Equation 4). Finally, a heat transfer equation is given by

$$a_{DB}\left(\frac{\rho_w |Q|}{\eta_w S^{1/2}} \right)^{4/5} k(\theta_w - \theta_i) = m\left[L + c_w(\theta_w - \theta_i) \right] \tag{6}$$

where the term on the LHS is an empirical expression for heat transfer at the ice conduit walls given a turbulent flow; this is obtained from an empirical relation among the Nusselt number, the Reynolds number, and the Prandtl number ([7]). Here $a_{DB} \sim 2$, η_w is the viscosity of water, and k is the thermal conductivity.

At the lake inlet, the "refilling" condition is given by

$$-\frac{A_L}{\rho_w g}\frac{\partial N}{\partial t} = m_L - Q \text{ at } x = 0 \tag{7}$$

where A_L is the (fixed) surface area of the lake and m_L is the geothermal melt rate in the caldera. That is, changes in the effective pressure at the seal are driven by the meltwater flux in the lake due to geothermal heating and the volumetric flux of water into the subglacial conduit. Here

$$\Phi = \rho_w g \sin\alpha - \frac{\partial p_i}{\partial x} \tag{8}$$

is the hydraulic gradient. These equations are nondimensionalized with

$$Q = Q_0 Q^*, \quad S = S_0 S^*, \quad p_i - p = N_0 N^*, \quad m = m_0 m^*, \quad x = l x^*, t = t_0 t^*, \quad \theta_w = \theta_i + \theta_0 \theta^*,$$

which gives

$$\frac{\partial S}{\partial t} = m - SN^n \tag{9a}$$

$$\epsilon\frac{\partial S}{\partial t} + \frac{\partial Q}{\partial x} = \epsilon r m + \Omega \tag{9b}$$

$$\Phi + \delta\frac{\partial N}{\partial x} = \frac{Q\,|Q|}{S^{8/3}} \tag{9c}$$

$$\epsilon S\frac{\partial \theta}{\partial t} + Q\frac{\partial \theta}{\partial x} = Q\left[\Phi + \delta\frac{\partial N}{\partial x}\right] - m(1+\epsilon r\theta) \tag{9d}$$

$$\theta\left(\frac{|Q|}{S^{1/2}}\right)^{0.8} = \gamma m(1+\epsilon r\theta) \tag{9e}$$

The nondimensional parameters are given by

$$\epsilon = \frac{\Phi_0 l}{\rho_i L} \tag{10a}$$

$$\delta = \frac{1}{\Phi_0 l}\left[\frac{Q_0^{1/4}\Phi_0^{11/8}}{\rho_i K L (f\rho_w g)^{3/8}}\right]^{\frac{1}{n}} \tag{10b}$$

$$\gamma = \frac{\rho_w c_w}{k a_{DB} l}\left(\frac{\eta_w}{\rho_w}\right)^{4/5} Q_0^{1/2}\left(\frac{f\rho_w g}{\Phi_0}\right)^{3/20} \tag{10c}$$

$$r = \frac{\rho_i}{\rho_w} \tag{10d}$$

$$\Omega = \frac{Ml}{Q_0} \tag{10e}$$

with the boundary condition

$$\frac{\partial N}{\partial t} = Q - \nu \text{ at } x = 0. \tag{11}$$

Reference values for these parameters are

$$\gamma \sim 2.5, \quad \epsilon \sim 0.05, \quad r \sim 0.9, \quad \delta \sim 0.22, \quad \Omega \sim 0.6 \cdot 10^{-3}. \tag{12}$$

(A table of physical parameter values used in the scaling is available in [4]). Ordinarily, flooding is initiated in the presence of the "seal" at the margin of the caldera. Now re-scale $x = \delta X$ to investigate near the boundary of the caldera, let $\omega = \delta\Omega$ and allow $\Phi < 0$ near the lake. Assume that ϵ and γ are small, which implies via Equation 9e that $\theta = 0$. The equation set then reduces to

$$\frac{\partial S}{\partial t} = \frac{|Q|^3}{S^{8/3}} - SN^n \tag{13a}$$

$$\frac{\partial Q}{\partial X} = \omega \tag{13b}$$

$$\Phi + \frac{\partial N}{\partial X} = \frac{Q\,|Q|}{S^{8/3}} \tag{13c}$$

with the boundary conditions

$$\frac{\partial N}{\partial t}(0,t) = Q(0,t) - \nu \text{ at } x = 0 \tag{14}$$

$$\frac{\partial N}{\partial X} \to 0 \text{ as } X \to \infty \tag{15}$$

where

$$\nu = \frac{m_L}{Q_0}. \tag{16}$$

Assume the following form for Φ,

$$\Phi = 1 - ae^{-bX}, \tag{17}$$

for some parameters a and b (which are related to the strength of the seal). Figure 3 shows the numerical solution of Equations 13a-13c and 14, which agrees quite reasonably with observations.

Note that in a steady state ($\partial S/\partial t = 0$) with $\Phi \sim 1$, Equations 13a-13c reduce to the Röthlisberger relation for N and Q.

1.2 Distributed drainage system

Massive flooding events have likely occurred beneath ice sheets such as Antarctica, with Lake Vostok potentially implicated. Note that flooding events beneath ice sheets are physically very different from events beneath glaciers, as drainage beneath ice sheets is not typically through Röthlisberger channels.

In Röthlisberger channels, N and Q are related via

$$N \sim \beta Q^{1/4n} \tag{18}$$

for a material parameter β. Under these circumstances, it is typical for a single conduit to develop, owing to the relationship between Q and N. If two Röthlisberger channels of differing radii are close together (such that water can escape from one channel to another through the bed), the channel with relatively small Q (small N, large p_w) will experience

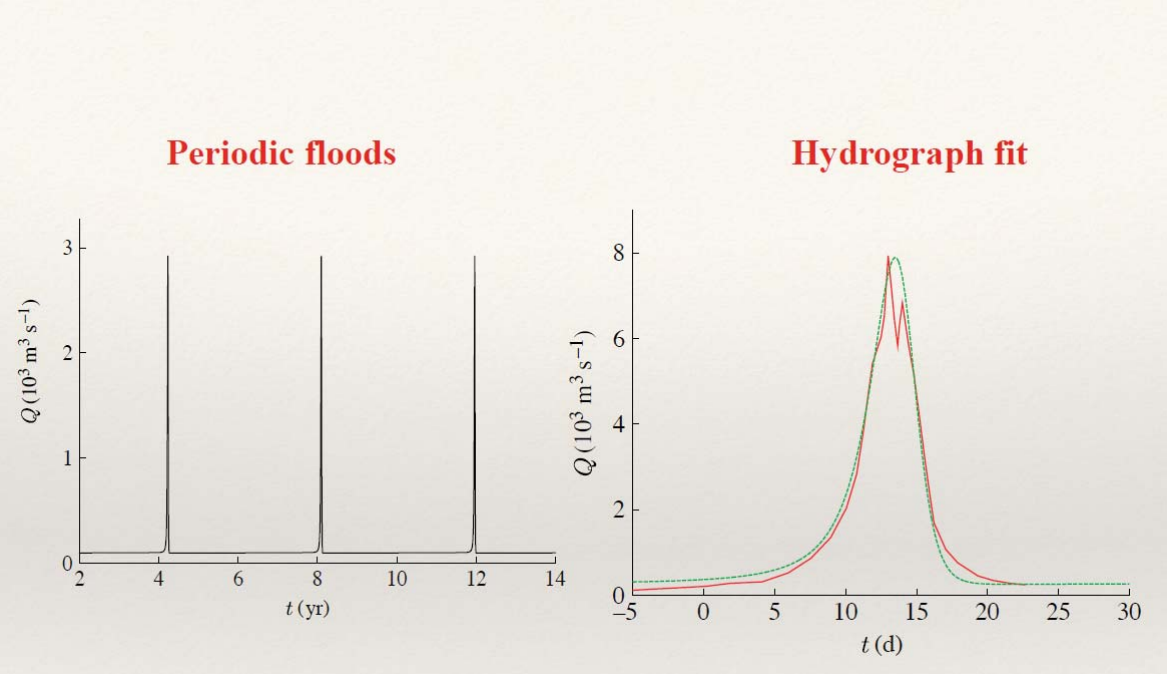

Figure 3: (a) Model showing periodic flooding at Grímsvötn. (b) Hydrograph of the observed (red) and modeled (green) discharge based upon the solution of Equations 13a-13c and 14 under the assumption that $a = 2.8, b = 4.316$. Figure adapted from [3].

leakage into the nearby channel of large Q, and the small channel will gradually close. If the subglacial sediment is relatively stiff, then it is possible for Röthlisberger channels to develop beneath a glacier. However, if sediment is significantly erodible, then it is likelier for a distributed drainage network to develop (rather than a single channel).

In prior derivations, Röthlisberger channels were assumed to be semi-circular with $h \sim w$, where w is the mean width and h is the mean depth. Now relax the assumption (as in the Röthlisberger theory) that $h \sim w$. Instead $R = S/l$, where R, the hydraulic radius, is a fraction of the cross section $S = wh$ and l, the wetted perimeter, and

$$w^2 = \frac{2^{4/3}\rho_w n'^2 Q^2}{\rho_i S_i h^{10/3}} \tag{19}$$

$$Kw^2 N^n = \frac{gS_i Q}{2L} \tag{20}$$

where n' a Manning roughness coefficient, K is related to the closure rate and is dependent upon the geometry, and S_i is the ice surface slope. This is a generalization of the Röthlisberger theory and reduces to it in the case $w \approx h$. It is derived from a Manning law and the assumption that the closure rate due to melting balances channel closure due to the ice overburden pressure. Assume that the channel depth is close to the critical depth at which sediment transport occurs. It then follows that

$$N = \frac{\gamma}{Q^{1/n}} \tag{21}$$

with

$$\gamma = \left[\frac{\rho_i g S_i^2 h_c^{10/3}}{2^{7/3} K L \rho_w n'^2} \right]^{1/n} \tag{22}$$

where h_c is a critical depth fixed by the critical stress for sediment transport and L is a function of the sliding velocity and effective pressure N. This suggests an inverse relationship between N and Q, unlike for Röthlisberger channels. Therefore, the closure mechanism discussed previously for Röthlisberger channels is avoided, which permits the existence of a distributed drainage network [7].

2 Subglacial Bedforms: Drumlins, Ribbed Moraine, and Mega-scale Glacial Lineations (MSGL)

The action of ice sheets during the last ice age has had profound effects on topography throughout the world. Ribbed moraines, drumlins, and Mega-Scale Glacial Lineations (MSGLs) (seen in Figures 4, 5, and 6, respectively) are prime examples of such effects. They are always seen in large clusters in areas of past glaciation (Sweden, Ireland, Canada), with the prime differences being the main direction of variation. Ribbed moraines, much like dunes, form transverse to the flow, while MSGLs are instead directed longitudinally. Drumlins, however, are fully three dimensional, being between these two extremes.

The glacial dynamics responsible for these features have not been settled. However, [6] has developed a model which couples ice sheet and deformable sediment dynamics, with a thin intermediate water film. This model exhibits all three of these formations, and we outline its development below.

2.1 Ice

We model the ice as a Newtonian fluid of viscosity η_i. The finite depth ice lies above a thin water layer, which in turn rests on a deformable bed of till (Figure 7). The inertial terms are negligible in the Navier-Stokes equations, giving Stokes flow

$$\nabla \cdot \boldsymbol{u} = 0, \tag{23}$$

$$0 = -\nabla P - \rho_i g \nabla z_i + \eta_i \nabla^2 \boldsymbol{u}, \tag{24}$$

where $\boldsymbol{u}$ is the ice velocity, ρ_i is the ice density, η_i is the dynamic viscosity, and P is the deviation from the cryostatic pressure.

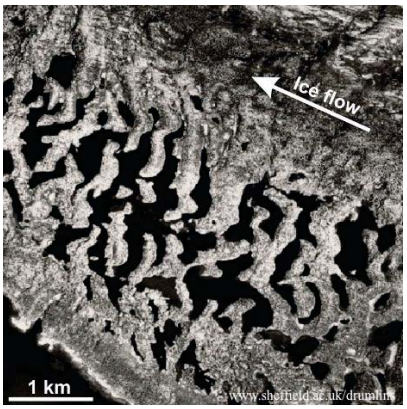

Figure 4: Ribbed moraines in lake Rogen, Sweden. Ridges form transverse to ice flow [6]. Figure adapted from https://www.sheffield.ac.uk /drumlins/rogen

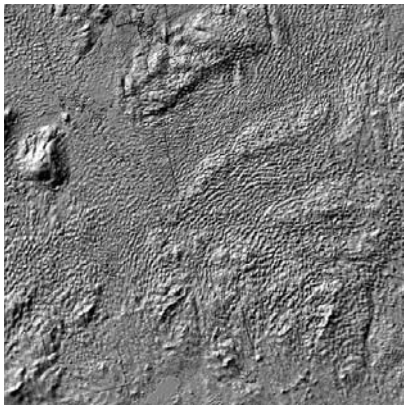

Figure 5: Digital elevation map of part of north central Ireland. The small bumps are drumlins, which are roughly 10 m high, and several hundred metres in length [6]. Figure adapted from [6].

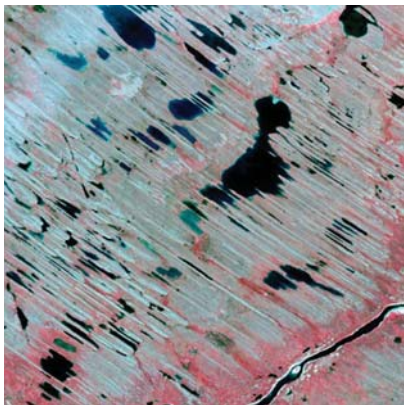

Figure 6: MSGLs in Canada, which are instead parallel to sheet flow [5]. Figure adapted from https://www.sheffield.ac.uk/ drumlins/msgl.

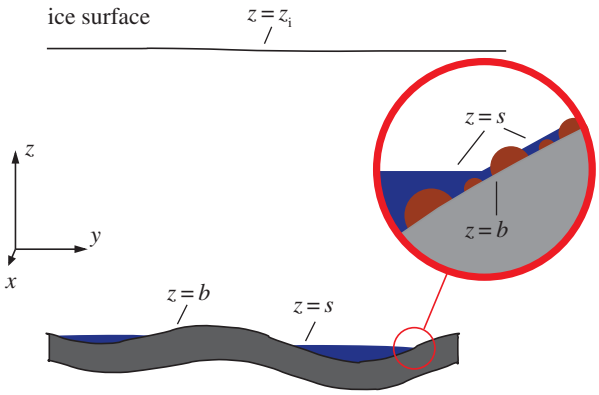

Figure 7: A view upstream of the model. The ice sheet, with upper surface $z = z_i$, rests on a water layer extending from $z = s$ to the sediment bed at $z = b$ [6]. Figure from [6].

At $z = z_i$ we specify matching normal stress τ_{nn}, with zero horizontal shear stress $\boldsymbol{\tau} = (\tau_{13}, \tau_{23})$

$$P - \tau_{nn} = 0, \tag{25}$$

$$\boldsymbol{\tau} = 0, \tag{26}$$

and additionally require a kinematic equation for w, which prescribes its value at the top boundary in terms of the ice sheet elevation z_i and the accumulation rate a

$$w = z_{i,t} + u z_{i,x} + v z_{i,y} - a. \tag{27}$$

At the bottom of the ice ($z = s$), we now require some relation for the shear stress. We assume it depends on the basal ice velocity u_b and the effective pressure at the interface

$N = p_i - p_w$,

$$\boldsymbol{\tau} = f(u_b, N)\frac{\boldsymbol{u}_b}{u_b}. \tag{28}$$

We specify a generalised Weertman sliding law for f

$$f(u_b, N) = RN^b u_b^c, \tag{29}$$

where R is the roughness coefficient, and b and c are the respective powers of the effective pressure N and basal velocity u_b. Finally, we have our second kinematic equation for w at the bottom boundary

$$w = s_t + us_x + vs_y. \tag{30}$$

2.2 Water

As mentioned, the water exists between the two interfaces, giving the layer thickness h as

$$h = s - b. \tag{31}$$

The hydraulic potential in the water is then

$$= \rho_i g(z_i - d_i) + \Delta\rho_{wi} gs - N + P - \tau_{nn}, \tag{32}$$

where $\Delta\rho_{wi} = \rho_w - \rho_i$ is the density difference between water and ice, and d_i is the ice depth, which is assumed to be constant over the smaller scale of the deformations we will observe.

The water between the ice and sediment is then modelled as a thin film. Its evolution is governed by Poiseuille-type flow

$$h_t = \nabla \cdot \left[\frac{h^3}{12\eta_w}\nabla\psi\right] + \Gamma. \tag{33}$$

Here, Γ represents sources due to ice melt (from geothermal heating, frictional heating, and heat flux into the ice).

2.3 Sediment

The sediment is also a deformable medium. However, unlike the water or ice, it will not deform until the basal stress applied to it by the ice $\tau = f(\bar{u}, N)$ exceeds the yield stress μN, where μ is the coefficient of friction. Hence, it will have a finite deformation depth h_A, below which the sediment is unperturbed, given by

$$h_A = \frac{[\tau/\mu - N]_+}{\Delta\rho_{sw}(1-\phi)g}, \tag{34}$$

(where $[y]_+ = \max\{y, 0\}$).

The governing conservation equation of the sediment is called the Exner equation, and models the change in the bed elevation b in terms of the sediment deformation depth h_A, an effective sediment viscosity η_s, and

$$b_t + \nabla \cdot \left[\frac{1}{2} u_0 \bar{u} h_A \boldsymbol{i} - \frac{h_A^3}{12\eta_s} \nabla N + Q(\tau_e) \frac{\boldsymbol{\tau}_e}{\tau_e} \right] = 0. \tag{35}$$

The first advective flux term represents shearing from the average ice flow $u_0\bar{u}$, where $\bar{u}$ is a spatial average of u at the base, defined so that $\overline{f(\bar{u}, N)} = \overline{f(u, N)}$. The second diffusive term then represents squeezing of the till in a thin layer h_A due to the effective pressure N. The final flux term represents sediment transport due to the effective stress $\boldsymbol{\tau}_e$ transmitted by the water to the bed, given by

$$\boldsymbol{\tau}_e = -\frac{1}{2} h \nabla \psi - \Delta\rho_{sw} g D_s \nabla b. \tag{36}$$

This is the actual viscous stress in the water plus a term related to the tendency of sediment to roll downhill, which depends on the difference in sediment and water density $\Delta\rho_{sw} = \rho_s - \rho_w$, and the average grain size of the sediment, D_s.

2.4 Reduced model

We can then non-dimensionalise this system, and significantly simplify the model. For more details on each step, please refer to [6].

Our upper ice equations are completely solvable in terms of the stress at the boundaries. By linearising the boundaries as constant, we can solve the upper system using the Fourier transform, defined to be

$$\hat{f}(k_x, k_y) = \int_{-\infty}^{\infty} \int_{-\infty}^{\infty} f(x, y) e^{ik_x x} e^{ik_y y} \, dx \, dy. \tag{37}$$

This leaves only the kinematic equation for w, which is now given by a Fourier convolution

$$w = \alpha s_t + \bar{u} s_x = J * \Phi, \tag{38}$$

where Φ represents a perturbation to the pressure, and J is given by the inverse transform of

$$\hat{J} = \frac{\sinh^2 j}{2k(j + \cosh j \sinh j)}, \qquad j = \frac{k}{\sigma}, \qquad k = \sqrt{k_x^2 + k_y^2}. \tag{39}$$

Here $\sigma = l_D/d_i$ is the ratio of the bedform length scale l_D to the ice depth scale d_i, and $\alpha = d_T/d_D$ is the ratio of the deformable till depth scale d_T to the bedform depth scale d_D. Finally, $\bar{u}(t)$ represents the x-averaged basal velocity, defined to give the average shear stress at the bed, which gives (when non-dimensionalised)

$$\overline{f(\bar{u}, N)} = 1, \quad \text{implying} \quad f(\bar{u}, N) = \frac{N^b}{\overline{N^b}}. \tag{40}$$

Our thin film evolution equation for the water depth simplifies considerably (throwing out small terms), to become

$$\nabla \cdot [h^3 \nabla \Psi] = \sigma \, h^3, \tag{41}$$

where

$$\Psi = s - N + \Phi, \tag{42}$$

can be thought of as akin to pressure in the water.

Our water thickness equation is given by

$$b = s - \delta h, \tag{43}$$

where $\delta = h_0/d_D$ is the ratio of the average film thickness to bedform depth scale.

Finally, our Exner equation simplifies to

$$b_t + \bar{u} A_x = \nabla \cdot [\beta A^3 \nabla N - \gamma B(\tau_e) \boldsymbol{\tau}_e]. \tag{44}$$

Here, A is a non-dimensional deformable till depth, given as

$$A = \frac{1}{2} \left[\frac{f(\bar{u}, N)}{\mu} - N \right]_+ . \tag{45}$$

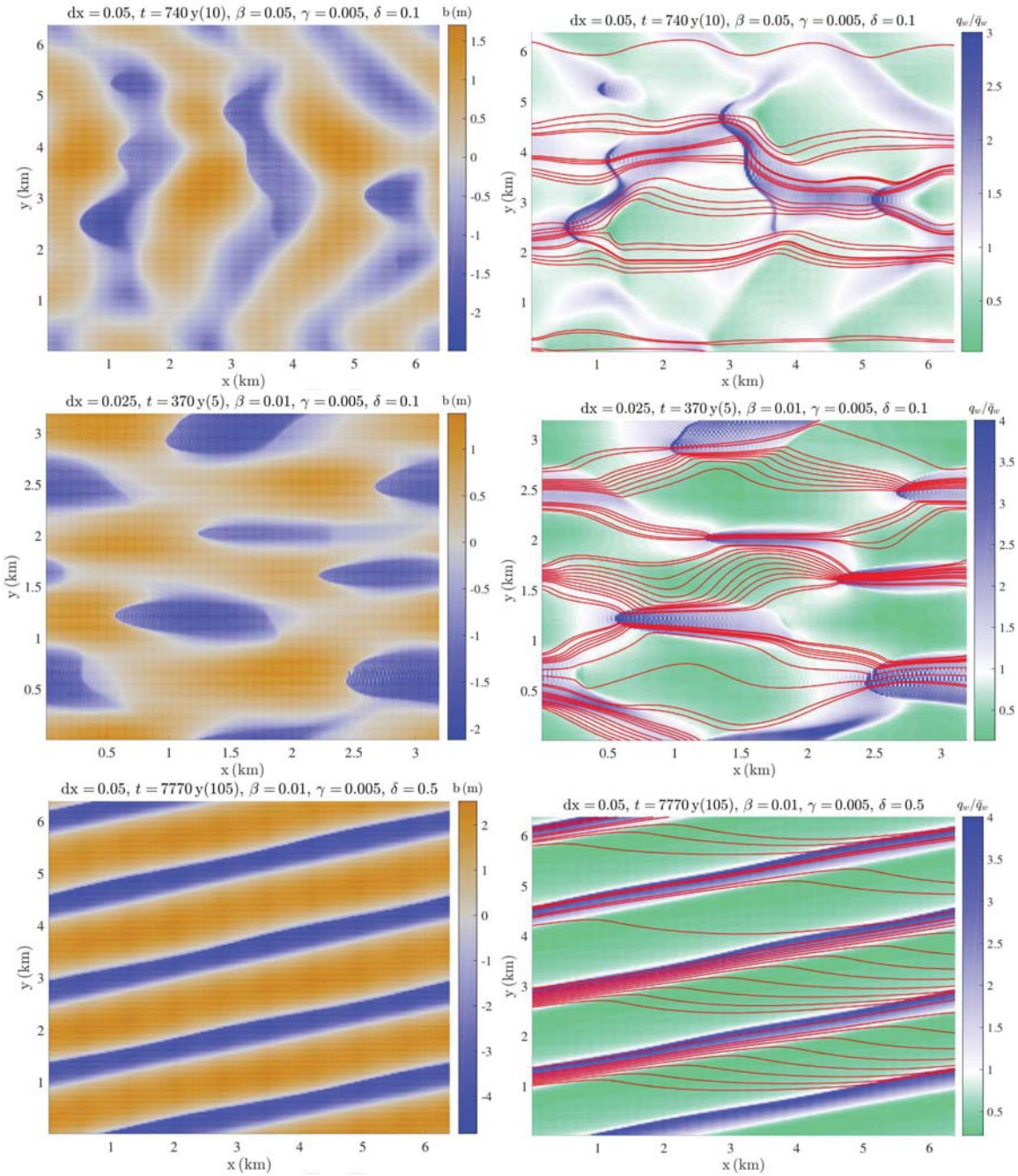

Figure 8: Simulations of the system on a periodic domain [2]. The left column shows topography and the right shows water flux, with red streamlines. Depending on the parameter choice, we can generate ribbed moraines, drumlins, or MSGLs. The incline of the MSGL stems from the periodicity of the domain, which does not enforce a direction of outflow. The chief numerical limit on the model is the smallness of δ. Figure adapted from [2].

The parameters β and γ are given by

$$\beta = \frac{2d_T}{3l_D}, \qquad \gamma = \frac{q_b}{d_T u_0} \tag{46}$$

where d_T is the scale of the deformable till depth, q_b is the scale of the sediment flux, and u_0 is the scale of the basal velocity. While small, both of these terms are necessary. The β term is required to stabilise the growth of the bedform, while the sediment transport γ term is required to generate the rilling instability responsible for MSGL formations. The advective $\bar{u}A$ term is responsible for the ribbing instability that generates the moraine formations. Finally, the stress $\boldsymbol{\tau}_e$ represents the effective stress of the water on the sediment, given by

$$\boldsymbol{\tau}_e = \sigma h \boldsymbol{i} - h\nabla\Psi. \tag{47}$$

Combined, we now have 8 unknowns, $\Psi, b, s, h, A, N, \boldsymbol{\tau}_e, \Phi$, but only 7 equations (numbered above). We therefore require an additional equation to close the system. We achieve this by specifying a relation between the height h and effective pressure N of the till.

The water film can be thought of as a porous layer. This porosity will decrease with the effective pressure, and increase with the film thickness. We then reason that the film thickness will be a decreasing function of effective pressure - if we squeeze harder, the layer thins.

To infer the scale of this process, consider some critical clast size h_c. If the film is thicker than this, the ice no longer rests on rocks jutting from the till, and the effective pressure drops to zero. If N changes by $O(N_0)$ when h changes by $O(h_c)$, then

$$-\frac{\partial N}{\partial h} \sim \frac{N_0 h_0}{\tau_b h_c} \equiv \frac{1}{\Lambda}, \tag{48}$$

where τ_b represents the basal stress scale. The simplest such relation satisfying these requirements is given by

$$\Lambda h N = 1. \tag{49}$$

Unsurprisingly, this is the least secure aspect of the model. However, when simulated, the model is able to recreate all three types of bedforms (Figure 8) by varying only three parameters.

References

[1] H. Björnsson, *Explanations of jökulhlaups from Grímsvötn, Vatnajökull, Iceland.*, 1974.

[2] J. S. Fannon, A. C. Fowler, and I. R. Moyles, *Numerical simulations of drumlin formation*, Proceedings of the Royal Society of London A: Mathematical, Physical and Engineering Sciences, 473 (2017).

[3] A. Fowler, *Dynamics of subglacial floods*, in Proceedings of the Royal Society of London A: Mathematical, Physical and Engineering Sciences, vol. 465, The Royal Society, 2009, pp. 1809–1828.

[4] A. Fowler, *Mathematical geoscience*, vol. 36, Springer Science & Business Media, 2011.

[5] A. C. Fowler, *The formation of subglacial streams and mega-scale glacial lineations*, Proceedings of the Royal Society of London A: Mathematical, Physical and Engineering Sciences, 466 (2010), pp. 3181–3201.

[6] A. C. Fowler and M. Chapwanya, *An instability theory for the formation of ribbed moraine, drumlins and mega-scale glacial lineations*, Proceedings of the Royal Society of London A: Mathematical, Physical and Engineering Sciences, 470 (2014).

[7] J. Nye, *Water flow in glaciers: jökulhlaups, tunnels and veins*, Journal of Glaciology, 17 (1976), pp. 181–207.